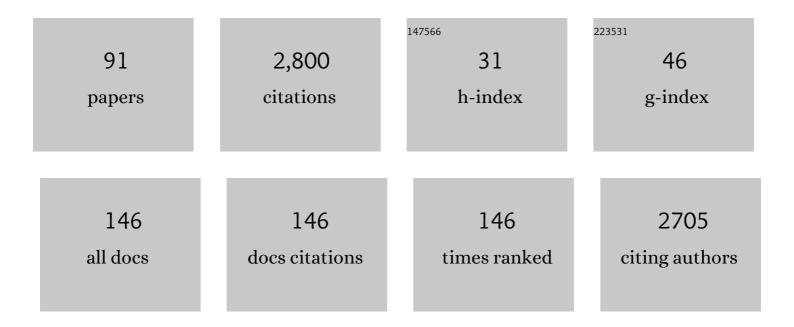
Patrick Chazette

List of Publications by Year in descending order

Source: https://exaly.com/author-pdf/5377501/publications.pdf Version: 2024-02-01



#	Article	IF	CITATIONS
1	Mesoscale spatio-temporal variability of airborne lidar-derived aerosol properties in the Barbados region during EUREC ⁴ A. Atmospheric Chemistry and Physics, 2022, 22, 1271-1292.	1.9	4
2	Wet deposition in the remote western and central Mediterranean as a source of trace metals to surface seawater. Atmospheric Chemistry and Physics, 2022, 22, 2309-2332.	1.9	10
3	EUREC ⁴ A observations from the SAFIRE ATR42 aircraft. Earth System Science Data, 2022, 14, 2021-2064.	3.7	9
4	Smoke in the river: an Aerosols, Radiation and Clouds in southern Africa (AEROCLO-sA) case study. Atmospheric Chemistry and Physics, 2022, 22, 5701-5724.	1.9	5
5	Preliminary range-resolved detection of stable water isotopologues by differential absorption lidar using a 2 Aµm parametric source. , 2022, , .		1
6	Experimental investigation of the stable water isotope distribution in an Alpine lake environment (L-WAIVE). Atmospheric Chemistry and Physics, 2021, 21, 10911-10937.	1.9	7
7	EUREC ⁴ A. Earth System Science Data, 2021, 13, 4067-4119.	3.7	88
8	A network of water vapor Raman lidars for improving heavy precipitation forecasting in southern France: introducing the WaLiNeAs initiative. Bulletin of Atmospheric Science and Technology, 2021, 2, 1.	0.4	5
9	Differential absorption lidar for water vapor isotopologues in the 1.98 µm spectral region: sensitivity analysis with respect to regional atmospheric variability. Atmospheric Measurement Techniques, 2021, 14, 6675-6693.	1.2	5
10	Mitigation of bias sources for atmospheric temperature and humidity in the mobile Raman Weather and Aerosol Lidar (WALI). Atmospheric Measurement Techniques, 2021, 14, 7525-7544.	1.2	5
11	Threeâ€dimensional pathways of dust over the Sahara during summer 2011 as revealed by new Infrared Atmospheric Sounding Interferometer observations. Quarterly Journal of the Royal Meteorological Society, 2020, 146, 2731-2755.	1.0	16
12	Remote sensing of two exceptional winter aerosol pollution events and representativeness of ground-based measurements. Atmospheric Chemistry and Physics, 2020, 20, 6749-6768.	1.9	7
13	Water vapor mixing ratio and temperature inter-comparison results in the framework of the Hydrological Cycle in the Mediterranean Experiment—Special Observation Period 1. Bulletin of Atmospheric Science and Technology, 2020, 1, 113-153.	0.4	9
14	Water vapor mixing ratio and temperature inter-comparison results in the framework of the Hydrological Cycle in the Mediterranean Experiment—Special Observation Period 1. , 2020, 1, 113.		1
15	Trade-wind clouds and aerosols characterized by airborne horizontal lidar measurements during the EUREC ⁴ A field campaign. Earth System Science Data, 2020, 12, 2919-2936.	3.7	13
16	Aerosol optical properties as observed from an ultralight aircraft over the Strait of Gibraltar. Atmospheric Measurement Techniques, 2020, 13, 4461-4477.	1.2	4
17	The AROME-WMED reanalyses of the first special observation period of the Hydrological cycle in the Mediterranean experiment (HyMeX). Geoscientific Model Development, 2019, 12, 2657-2678.	1.3	12
18	Accuracy of current Arctic springtime water vapour estimates, assessed by Raman lidar. Quarterly Journal of the Royal Meteorological Society, 2019, 145, 1234-1249.	1.0	8

#	Article	IF	CITATIONS
19	Transport of aerosols over the French Riviera – link between ground-based lidar and spaceborne observations. Atmospheric Chemistry and Physics, 2019, 19, 3885-3904.	1.9	6
20	The Aerosols, Radiation and Clouds in Southern Africa Field Campaign in Namibia: Overview, Illustrative Observations, and Way Forward. Bulletin of the American Meteorological Society, 2019, 100, 1277-1298.	1.7	59
21	Evidence of the complexity of aerosol transport in the lower troposphere on the Namibian coast during AEROCLO-sA. Atmospheric Chemistry and Physics, 2019, 19, 14979-15005.	1.9	12
22	Preliminary results from the FARCE 2015 campaign: multidisciplinary study of the forest–gas–aerosol–cloud system on the tropical island of La Réunion. Atmospheric Chemistry and Physics, 2019, 19, 10591-10618.	1.9	16
23	Impact of biomass burning on pollutant surface concentrations in megacities of the Gulf of Guinea. Atmospheric Chemistry and Physics, 2018, 18, 2687-2707.	1.9	36
24	Analysis of a warehouse fire smoke plume over Paris with an N ₂ Raman lidar and an optical thickness matching algorithm. Atmospheric Measurement Techniques, 2018, 11, 6525-6538.	1.2	3
25	Optical properties of an industrial fire observed with a ground based N2-Raman lidar over the Paris area. EPJ Web of Conferences, 2018, 176, 04006.	0.1	Ο
26	Multiâ€scale observations of atmospheric moisture variability in relation to heavy precipitating systems in the northwestern Mediterranean during HyMeX IOP12. Quarterly Journal of the Royal Meteorological Society, 2018, 144, 2761-2780.	1.0	12
27	Springtime aerosol load as observed from ground-based and airborne lidars over northern Norway. Atmospheric Chemistry and Physics, 2018, 18, 13075-13095.	1.9	8
28	Aerosol distribution in the northern Gulf of Guinea: local anthropogenic sources, long-range transport, and the role of coastal shallow circulations. Atmospheric Chemistry and Physics, 2018, 18, 12363-12389.	1.9	21
29	Atmospheric aerosol variability above the Paris Area during the 2015 heat wave - Comparison with the 2003 and 2006 heat waves. Atmospheric Environment, 2017, 170, 216-233.	1.9	17
30	Springtime major pollution events by aerosol over Paris Area: From a case study to a multiannual analysis. Journal of Geophysical Research D: Atmospheres, 2017, 122, 8101-8119.	1.2	9
31	EUREC4A: A Field Campaign to Elucidate the Couplings Between Clouds, Convection and Circulation. Surveys in Geophysics, 2017, 38, 1529-1568.	2.1	132
32	Raman Lidar Observations of Aerosol Optical Properties in 11 Cities from France to Siberia. Remote Sensing, 2017, 9, 978.	1.8	18
33	Mini N2-Raman Lidar Onboard Ultra-Light Aircraft for Aerosol Measurements: Demonstration and Extrapolation. Remote Sensing, 2017, 9, 1226.	1.8	11
34	EUREC4A: A Field Campaign to Elucidate the Couplings Between Clouds, Convection and Circulation. Space Sciences Series of ISSI, 2017, , 357-396.	0.0	2
35	Calibration of a water vapour Raman lidar with a kite-based humidity sensor. Atmospheric Measurement Techniques, 2016, 9, 1083-1094.	1.2	9
36	Airborne UV Lidar for Forest Parameter Retrievals. EPJ Web of Conferences, 2016, 119, 22006.	0.1	0

#	Article	IF	CITATIONS
37	Intense Particulate Pollution Events Observed with Lidar over the Paris Megalopolis. EPJ Web of Conferences, 2016, 119, 23010.	0.1	Ο
38	Principle and Physics of the LiDAR Measurement. , 2016, , 201-247.		13
39	Tropical Forests of Réunion Island Classified from Airborne Full-Waveform LiDAR Measurements. Remote Sensing, 2016, 8, 43.	1.8	6
40	A multiâ€instrument and multiâ€model assessment of atmospheric moisture variability over the western Mediterranean during HyMeX. Quarterly Journal of the Royal Meteorological Society, 2016, 142, 7-22.	1.0	16
41	Exceptional aerosol pollution plume observed using a new ULA-lidar approach. Atmospheric Environment, 2016, 141, 470-480.	1.9	6
42	Temporal consistency of lidar observations during aerosol transport events in the framework of the ChArMEx/ADRIMED campaign at Minorca in June 2013. Atmospheric Chemistry and Physics, 2016, 16, 2863-2875.	1.9	30
43	Overview of the Chemistry-Aerosol Mediterranean Experiment/Aerosol Direct Radiative Forcing on the Mediterranean Climate (ChArMEx/ADRIMED) summer 2013 campaign. Atmospheric Chemistry and Physics, 2016, 16, 455-504.	1.9	110
44	Long-range transport and mixing of aerosol sources during the 2013 North American biomass burning episode: analysis of multiple lidar observations in the western Mediterranean basin. Atmospheric Chemistry and Physics, 2016, 16, 4725-4742.	1.9	54
45	Tropical moisture enriched storm tracks over the Mediterranean and their link with intense rainfall in the Cevennesâ€Vivarais area during HyMeX. Quarterly Journal of the Royal Meteorological Society, 2016, 142, 320-334.	1.0	21
46	The radiative impact of desert dust on orographic rain in the Cévennes–Vivarais area: a case study from HyMeX. Atmospheric Chemistry and Physics, 2015, 15, 12231-12249.	1.9	7
47	Lidar profiling of aerosol optical properties from Paris to Lake Baikal (Siberia). Atmospheric Chemistry and Physics, 2015, 15, 5007-5026.	1.9	30
48	End-to-End Simulation for a Forest-Dedicated Full-Waveform Lidar Onboard a Satellite Initialized from Airborne Ultraviolet Lidar Experiments. Remote Sensing, 2015, 7, 5222-5255.	1.8	9
49	Influence of an urban canopy model and PBL schemes on vertical mixing for air quality modeling over Greater Paris. Atmospheric Environment, 2015, 107, 289-306.	1.9	37
50	Interest of a Full-Waveform Flown UV Lidar to Derive Forest Vertical Structures and Aboveground Carbon. Forests, 2014, 5, 1454-1480.	0.9	23
51	The mobile Water vapor Aerosol Raman LIdar and its implication in the framework of the HyMeX and ChArMEx programs: application to a dust transport process. Atmospheric Measurement Techniques, 2014, 7, 1629-1647.	1.2	49
52	Modelling and assimilation of lidar signals over Greater Paris during the MEGAPOLI summer campaign. Atmospheric Chemistry and Physics, 2014, 14, 3511-3532.	1.9	28
53	Comparison of IASI water vapor retrieval with H ₂ O-Raman lidar in the framework of the Mediterranean HyMeX and ChArMEx programs. Atmospheric Chemistry and Physics, 2014, 14, 9583-9596.	1.9	28
54	Assimilation of lidar signals: application to aerosol forecasting in the western Mediterranean basin. Atmospheric Chemistry and Physics, 2014, 14, 12031-12053.	1.9	44

#	Article	IF	CITATIONS
55	Evaluation of the Weather Research and Forecast/Urban Model Over Greater Paris. Boundary-Layer Meteorology, 2013, 149, 105-132.	1.2	61
56	Assimilation of ground versus lidar observations for PM ₁₀ forecasting. Atmospheric Chemistry and Physics, 2013, 13, 269-283.	1.9	36
57	Airborne measurements of trace gases and aerosols over the London metropolitan region. Atmospheric Chemistry and Physics, 2012, 12, 5163-5187.	1.9	43
58	Eyjafjallajökull ash concentrations derived from both lidar and modeling. Journal of Geophysical Research, 2012, 117, .	3.3	51
59	Comparison of lidar-derived PM ₁₀ with regional modeling and ground-based observations in the frame of MEGAPOLI experiment. Atmospheric Chemistry and Physics, 2011, 11, 10705-10726.	1.9	50
60	Potential of an ultraviolet, medium-footprint lidar prototype for retrieving forest structure. ISPRS Journal of Photogrammetry and Remote Sensing, 2011, 66, S92-S102.	4.9	8
61	Aerosol content survey by mini N2-Raman lidar: Application to local and long-range transport aerosols. Atmospheric Environment, 2011, 45, 7487-7495.	1.9	38
62	Radiative heating rates profiles associated with a springtime case of Bodélé and Sudan dust transport over West Africa. Atmospheric Chemistry and Physics, 2010, 10, 8131-8150.	1.9	60
63	Synergy between CALIOP and MODIS instruments for aerosol monitoring: application to the Po Valley. Atmospheric Measurement Techniques, 2010, 3, 893-907.	1.2	29
64	Parisfog. Bulletin of the American Meteorological Society, 2010, 91, 767-783.	1.7	120
65	Observing the Forest Canopy with a New Ultra-Violet Compact Airborne Lidar. Sensors, 2010, 10, 7386-7403.	2.1	16
66	Simultaneous observations of lower tropospheric continental aerosols with a groundâ€based, an airborne, and the spaceborne CALIOP lidar system. Journal of Geophysical Research, 2010, 115, .	3.3	35
67	Particulate contribution to extinction of visible radiation: Pollution, haze, and fog. Atmospheric Research, 2009, 92, 443-454.	1.8	105
68	Assessment of vertically-resolved PM ₁₀ from mobile lidar observations. Atmospheric Chemistry and Physics, 2009, 9, 8617-8638.	1.9	62
69	Validation of aerosol and cloud layer structures from the space-borne lidar CALIOP using a ground-based lidar in Seoul, Korea. Atmospheric Chemistry and Physics, 2008, 8, 3705-3720.	1.9	132
70	Radiative budget in the presence of multi-layered aerosol structures in the framework of AMMA SOP-0. Atmospheric Chemistry and Physics, 2008, 8, 6839-6864.	1.9	43
71	Vertical profiles of urban aerosol complex refractive index in the frame of ESQUIF airborne measurements. Atmospheric Chemistry and Physics, 2008, 8, 901-919.	1.9	46
72	Retrieval of aerosol complex refractive index from a synergy between lidar, sunphotometer and in situ measurements during LISAIR experiment. Atmospheric Chemistry and Physics, 2007, 7, 2797-2815.	1.9	62

#	Article	IF	CITATIONS
73	New Approach for Aerosol Profiling with a Lidar Onboard an Ultralight Aircraft: Application to the African Monsoon Multidisciplinary Analysis. Environmental Science & Technology, 2007, 41, 8335-8341.	4.6	71
74	Surface and aerodynamic roughness in arid and semiarid areas and their relation to radar backscatter coefficient. Journal of Geophysical Research, 2006, 111, n/a-n/a.	3.3	74
75	Three-dimensional survey of pollution during winter in French Alps valleys. Atmospheric Environment, 2005, 39, 1035-1047.	1.9	45
76	Experimental and theoretical studies of the aureole about a point source that is due to atmospheric scattering in the middle ultraviolet. Applied Optics, 2005, 44, 1250.	2.1	9
77	Optical properties of urban aerosol from airborne and ground-based in situ measurements performed during the Etude et Simulation de la Qualité de l'air en Ile de France (ESQUIF) program. Journal of Geophysical Research, 2005, 110, .	3.3	52
78	Measurements of stratospheric volcanic aerosol optical depth from NOAA TIROS Observational Vertical Sounder (TOVS) observations. Journal of Geophysical Research, 2004, 109, n/a-n/a.	3.3	4
79	The monsoon aerosol extinction properties at Goa during INDOEX as measured with lidar. Journal of Geophysical Research, 2003, 108, .	3.3	70
80	A synthesis of the Air Pollution Over the Paris Region (ESQUIF) field campaign. Journal of Geophysical Research, 2003, 108, .	3.3	54
81	Variational method for the retrieval of the optical thickness and the backscatter coefficient from multiangle lidar profiles. Applied Optics, 2002, 41, 493.	2.1	37
82	Determination by spaceborne backscatter lidar of the structural parameters of atmospheric scattering layers. Applied Optics, 2001, 40, 3428.	2.1	26
83	Cloud filter for CO retrieval from IMG infrared spectra using ECMWF temperatures and POLDER cloud data. Geophysical Research Letters, 2001, 28, 2397-2400.	1.5	22
84	A case study of optical and chemical ground apportionment for urban aerosols in Thessaloniki. Atmospheric Environment, 2001, 35, 2497-2506.	1.9	70
85	Lidar and satellite retrieval of dust aerosols over the Azores during SOFIA/ASTEX. Atmospheric Environment, 2001, 35, 4297-4304.	1.9	31
86	Airborne lidar measurements of aerosol spatial distribution and optical properties over the Atlantic Ocean during a European pollution outbreak of ACE-2. Tellus, Series B: Chemical and Physical Meteorology, 2000, 52, 662-677.	0.8	34
87	Airborne lidar measurements of aerosol spatial distribution and optical properties over the Atlantic Ocean during a European pollution outbreak of ACE-2. Tellus, Series B: Chemical and Physical Meteorology, 2000, 52, 662-677.	0.8	27
88	Retrieval and monitoring of aerosol optical thickness over an urban area by spaceborne and ground-based remote sensing. Applied Optics, 1999, 38, 6918.	2.1	18
89	Direct estimate of methane radiative forcing by use of nadir spectral radiances. Applied Optics, 1998, 37, 3113.	2.1	8
90	Potential use of spaceborne lidar measurements to improve atmospheric temperature retrievals from passive sensors. Applied Optics, 1998, 37, 7670.	2.1	3

#	Article	IF	CITATIONS
91	Wind speed dependence of atmospheric boundary layer optical properties and ocean surface reflectance as observed by airborne backscatter lidar. Journal of Geophysical Research, 1998, 103, 25137-25158.	3.3	32